

Behavioral performance during vibration and shock for a tactical grade IMU

R. Holm, H. Schou, H. R. Petersen, M. Horntvedt

Sensor AS,
Knudsrodveien 7
P.O.Box 1004
3194 Horten
NORWAY

Abstract

Sensoror has since 2009 produced tactical-grade MEMS-based IMUs and gyro-clusters. During this time, approximately 25,000 parts, containing 75,000 MEMS gyros, have been shipped. Sensoror has earlier been a supplier of high-reliable MEMS sensors, including gyros, to the demanding safety applications in the automotive industry for more than 20 years.

The MEMS gyro in Sensoror's IMUs and gyro-clusters was originally designed to function in a high-vibration environment for roll-over detection in cars. Its well-proven differential Butterfly-structure with a balanced resonating element, operating in vacuum to achieve a high Q-factor, inherently provides high robustness towards vibration and shock compared to traditional FOGs and RLGs.

This paper focuses on the MEMS gyros and present data prior to, during and after being exposed to several vibration profiles and shocks. The selected vibration profiles cover both steady state sinusoidal and random-vibration spectra used in the characterization of a wide variety of applications like aircrafts, smart munition and missiles. Applied shocks are in the range of 40g to 1500g. In addition to extracting key-data like VRC, time-analyses of the data are presented, covering the signals themselves and the behavior of the continuously running self-diagnostic feature implemented in the IMUs.

Data is presented for 8 IMUs (24 gyros) in order to provide information about spread in the investigated properties.

1. Short summary of the history of Sensoror

Sensoror was founded in 1985 as a spin-out company of the Norwegian company AME (Aker Mikro Elektronikk). Its MEMS-technology had been specifically developed with high-reliability in mind, and Sensoror's products were well established within the demanding fields of medical, aerospace and military. During the first two decades, Sensoror had its focus on the automotive segment, delivering more than 35 million accelerometers to airbag applications, more than 250 million pressure sensors and accelerometers to tire-pressure applications and more than 2 million gyros to roll-over applications. Sensoror was certified and in compliance with all relevant and required quality standards and gained through this period solid experience and mind-set of high-volume production of products with safety and high-reliability requirements. From 2009, Sensoror changed its focus to high-precision, tactical-grade 3-axis gyro-modules (STIM202 and STIM210) and IMUs

(STIM300), addressing the segment of high-precision gyros typically covered by fiber-optic gyros. The new products were all based on the technology and know-how established during the previous two decades of high-volume production and deliveries to highly demanding applications.

2. Gyro sensing element

The Sensoror gyro sensing element was originally developed for roll-over detection in cars, an application requiring robustness and reliability. It is simple in its structure, consisting of two proof masses suspended by three springs and 4 sets of electrodes to enable differential drive and detection, as shown in figure 1:

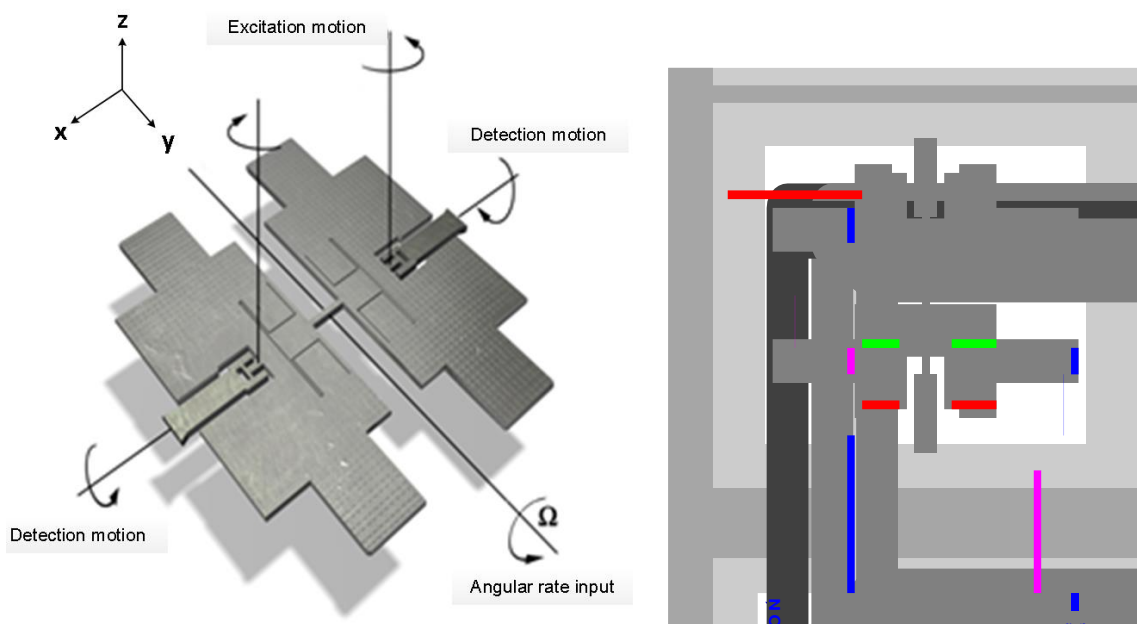


Figure 1: The Sensoror gyro sensing element (left) and capacitor lay-out (right)

The gyro sensing element is made of monocrystalline silicon, a material with no properties of fatigue leading to superior reliability. Each proof-mass weighs only $\sim 20\mu\text{grams}$. Combined with its simplicity, this makes the Sensoror gyro sensing element very robust towards g-forces.

3. Continuous self-test

Having successfully supplied products to safety-critical applications like airbags and roll-over, this has made a big impact in the design-philosophy at Sensoror. Topics like self-test during operation and signal integrity are a natural part of the development process.

The gyro sensing elements are driven at their respective resonances. By continuously monitoring parameters like resonance-frequency and -amplitude, the result is a continuous

self-test covering the proof masses, their free movement and the integrity of drive- and detection-electrodes. The status of the self-test is transmitted with each data-package and will during the vibrations and shocks be inspected to verify whether the operation of the gyros has been affected by the applied stimuli.

4. Axis definitions and nomenclature

As vibrations and shocks have been applied in several directions, there is a need to define the different axes of the IMU. Each IMU consists of three gyros, measuring the rotational speeds around the three axes of the IMU. The gyro sensing elements are for obvious reasons mounted in different orientations inside the IMU and will therefore individually experience the applied stimulus in different directions. The definition of axis-directions for the IMU and the internal gyro sensing elements is shown in figure 2:

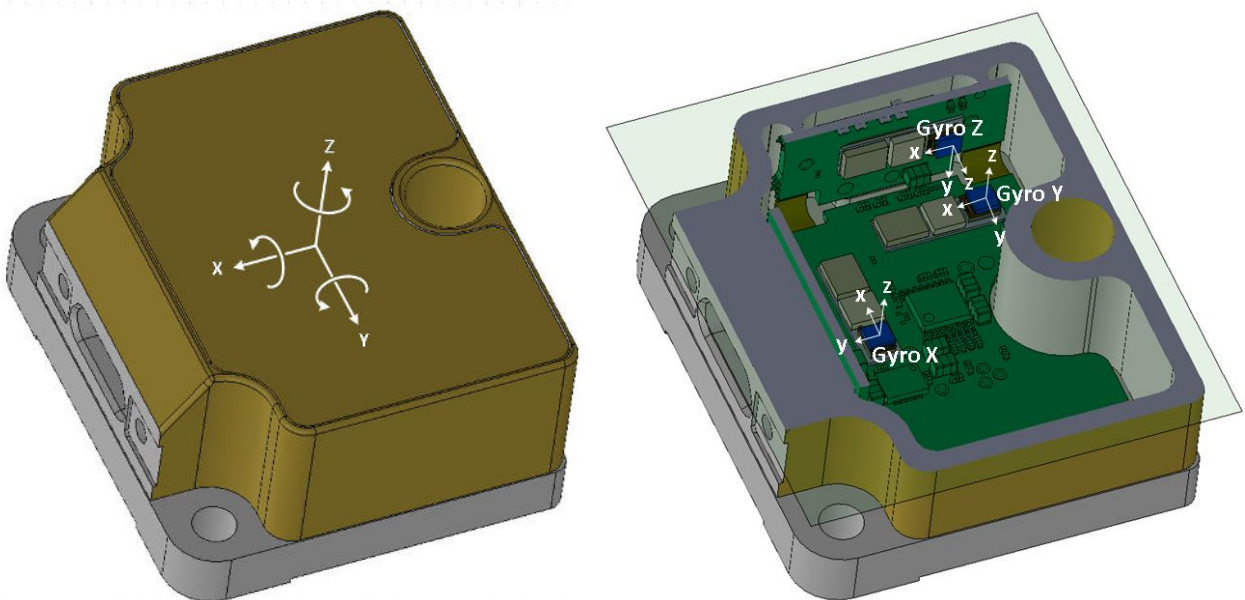


Figure 2: Axis-direction of IMU (left) and gyro sensing elements (right)

Nomenclature:

- "Vib_x" is vibration in X-direction. Similar for other axes
- "Gyro X" is the gyro measuring rotation around the IMUs X-axis. Similar for other axes
- "Vib_Gx" is vibration in the individual gyro's x-direction as defined in figure 2. Similar for other axes
- Shock_X is shock in the X-direction. Similar for other axes

5. Vibration Tests

In this study, both sinusoidal and random vibrations have been applied to investigate the impact on the gyros used in STIM210 and STIM300. The sinusoidal vibration tests were performed at steady state conditions at different amplitudes and frequencies as presented in table 1.

The random vibrations were performed according to MIL-STD 810E 514.4 "High Performance Aircraft".

The gyros were configured as follows:

- Range = $\pm 400^\circ/\text{s}$, output being clipped at $\pm 480^\circ/\text{s}$
- Sampling rate = 2000Hz
- Low-pass filter = 33Hz
- Data transmission rate = 250Hz

5.1 Sinusoidal steady state vibrations:

24 gyros (8 IMUs) have been characterized with the purpose of calculating the Vibration Rectification Coefficient (VRC), a DC-shift observed due to non-linear effects when being exposed to vibrations.

The following test matrix was applied:

Direction of vibration	Amplitude [g] peak	Frequency [Hz]
X, Y, Z	5, 10, 20	55, 500, 1000, 1500, 2000

Table 1: Test matrix for sinusoidal vibrations

The following test sequence was applied for each combination of amplitude/frequency (ref. figure 3):

- No vibration applied:10min
- Vibration:10min
- No vibration applied:10min
- Vibration:10min
- No vibration applied:10min
- Calculate average of the individual test sections
- Calculate VRC according to equation 1

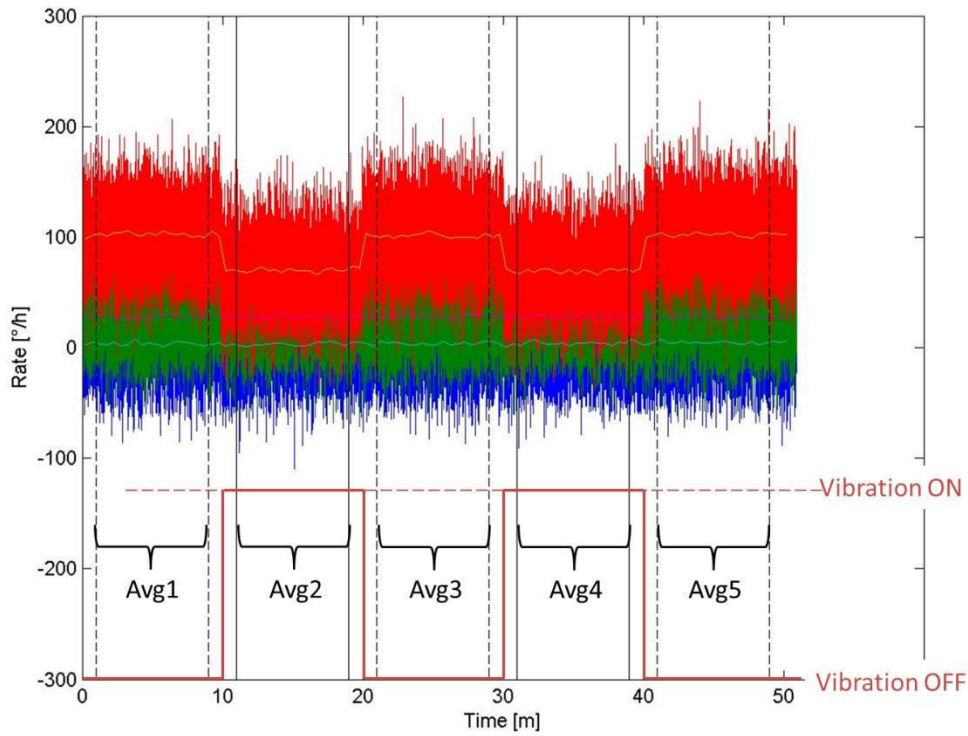


Figure 3: Example of a sinusoidal vibration test

$$VRC = ABS \left[\frac{(Avg2 - Avg1) + (Avg2 - Avg3) + (Avg4 - Avg3) + (Avg4 - Avg5)}{4 g_{rms}^2} \right] [^{\circ}/h/g_{rms}^2]$$

Equation 1: Calculation of VRC

The mean of VRCs measured in any direction and any gyro as function of frequency and amplitude is summarized in figure 4 and histograms for each combination of frequency and amplitude can be found in figure 5.

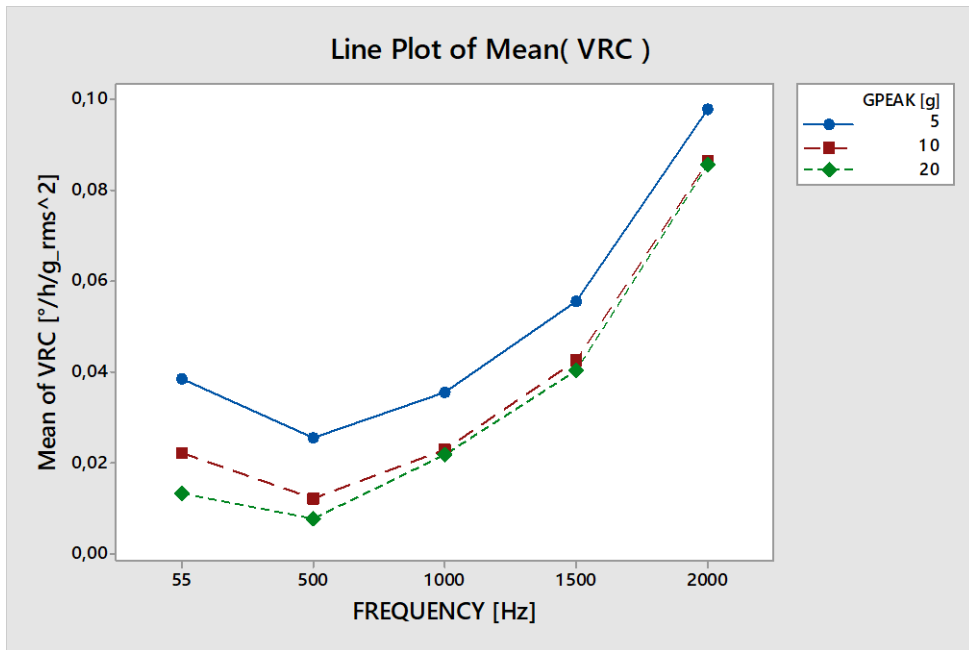


Figure 4: Main summary of sinusoidal vibration tests

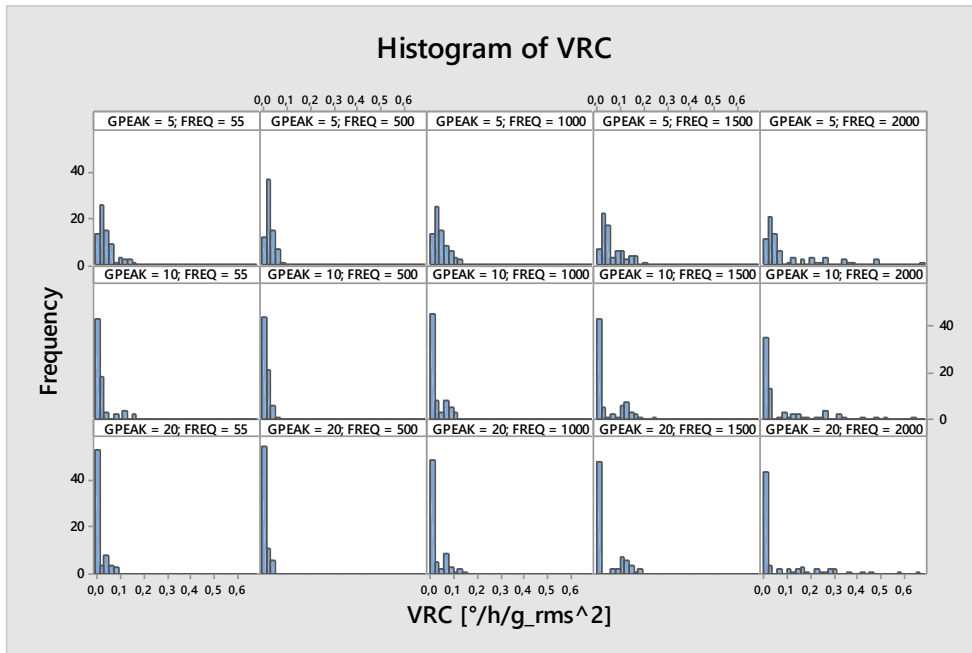


Figure 5: Distributions at each amplitude and frequency

No error reporting from the continuous self-test was observed during any of these tests.

Some of the distributions shown in figure 5 display a double distribution, e.g. the histogram for 10g and 1500Hz. This could be explained by the gyro sensing element having different vibration sensitivity dependent on the direction of the vibration. In figure 6, the VRC has been plotted towards the axis-direction of the gyro sensing elements.

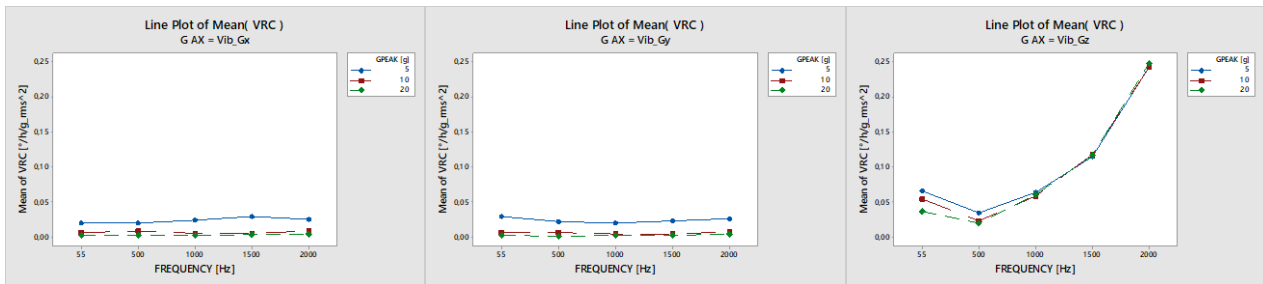


Figure 6: VRCs measured in the different directions of the gyro sensing elements

Figure 6 clearly shows that only the z-direction of the gyro sensing element is sensitive to vibration. Referring back to the design of the gyro sensing element, ref. figure 1, this is quite as expected as a g-force in the z-direction would directly affect the capacitances formed by the proof masses and the electrodes used for drive and sense.

As the gyro sensing elements have two insensitive directions, it is worth investigating if there is an axis on IMU-level where all the gyro sensing elements are insensitive. In figure 7, the VRCs have been plotted as function of vibration-direction both with respect to IMU and gyro sensing element.

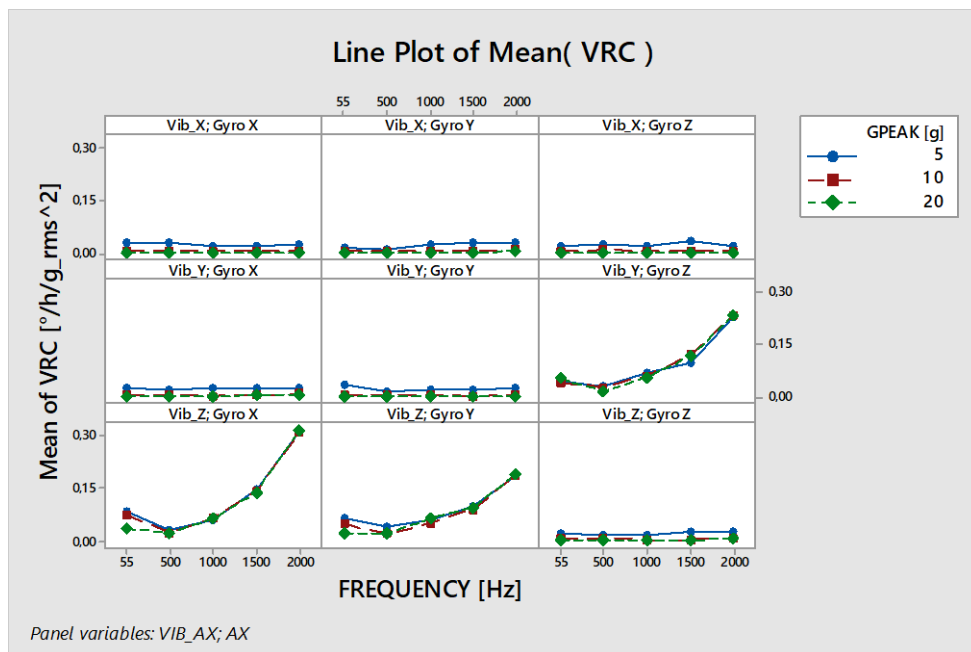


Figure 7: VRCs measured when applying vibration in different directions

Indeed, figure 7 shows that when vibration is applied in the x-direction of the IMU, all axes are insensitive to vibration.

For frequencies up to 500Hz, all axes are insensitive to vibration or the sensitivity is below the detection-level of the measurements presented.

Figure 8 shows the cumulative distribution frequency (CDF) plot for the VRC when vibration is applied in the sensitive direction of the gyro sensing elements at frequencies from 500Hz and above. Mean + 1 sigma values have been marked in the plot:

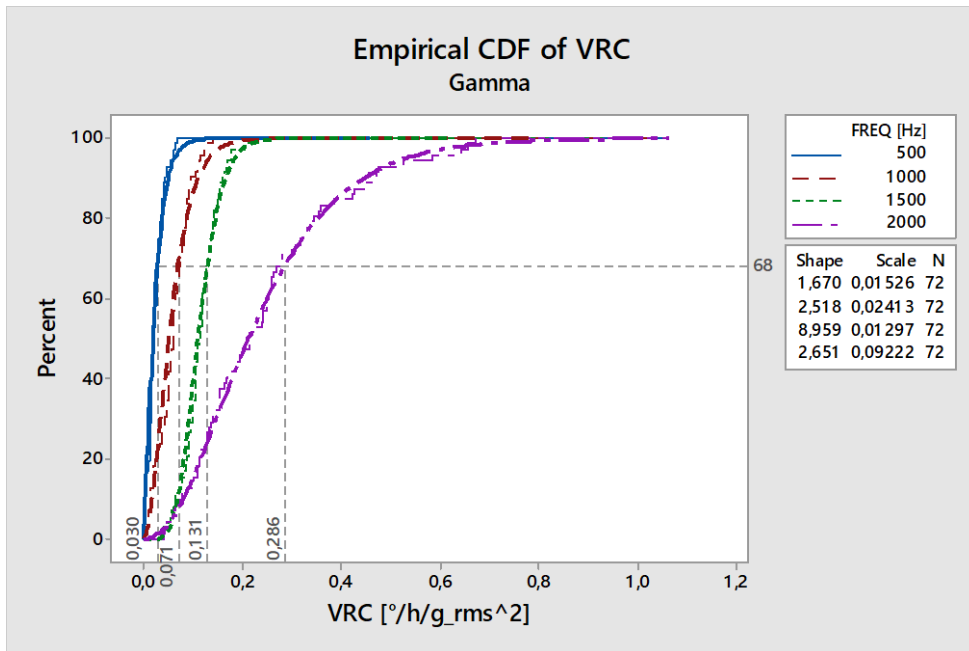


Figure 8: CDF of VRC when vibration is applied in the z-direction of the gyro sensing element

5.2 Random vibrations

The VRC of 24 gyros (8 IMUs) were measured using random vibrations according to MIL STD 810E 514.4 "High Performance Aircraft". The spectrum ($g_{rms}=14.83$) is specified in Figure 9. The vibrations were applied in all three axis-directions.

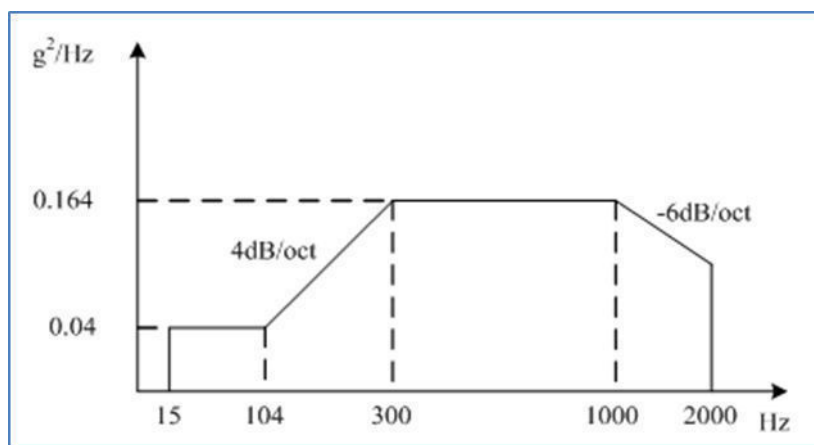


Figure 9: Vibration spectrum: "High Performance Aircraft"

Test Sequence:

- No vibration applied:15min
- Vibration:15min
- No vibration applied:15min
- Vibration:15min
- No vibration applied:15min
- Calculate average of the individual test sections
- Calculate VRC according to equation 1 (same method as for the sinusoidal vibrations)

Figure 10 shows the applied spectrum during the tests:

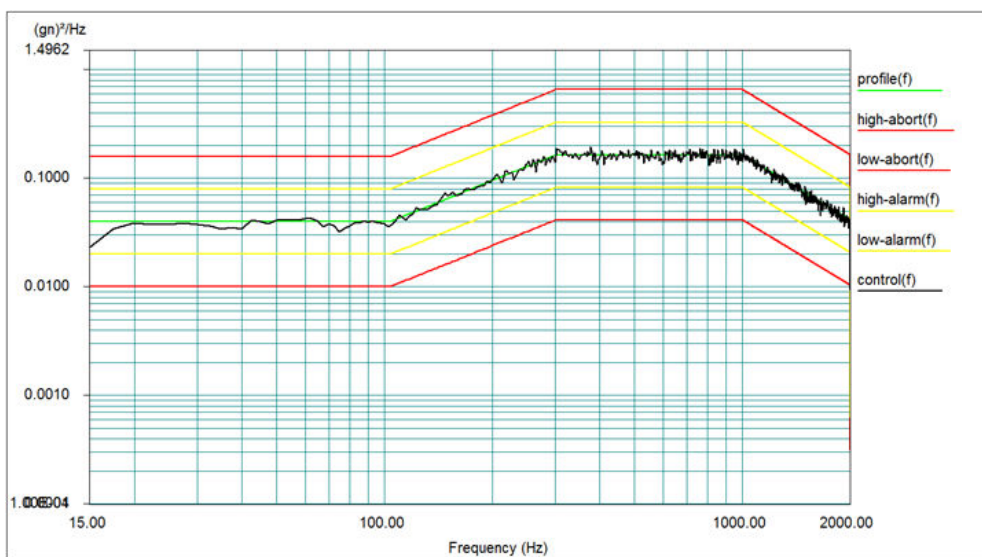


Figure 10: Spectrum monitored during test

The histogram in figure 11 summarizes the measured VRCs from the random vibration test:

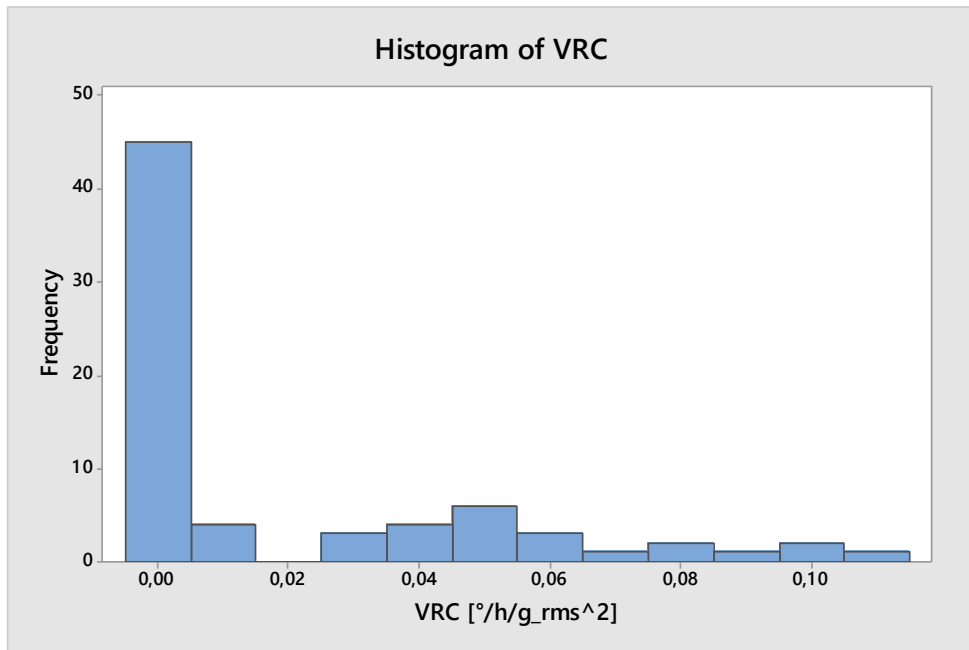


Figure 11: Distribution of VRC from random vibrations

No error reporting from the continuous self-test was observed during any of these tests.

The histogram in figure 11 shows a double-distribution and so a similar analysis, as was done for the sinusoidal vibration test, should be performed to check whether the vibration sensitivity is different in axes as defined by the gyro sensing element. Figure 12 shows the result of this analysis:

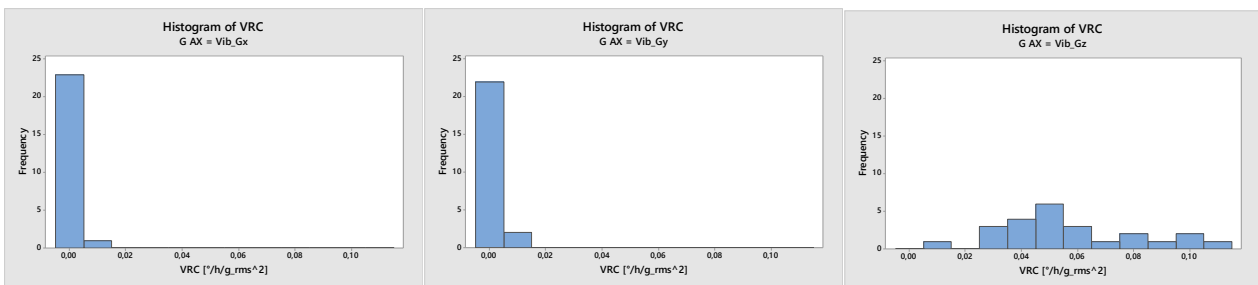


Figure 12: Distribution of VRC in the axes of the gyro sensing element

As expected, the gyro sensing element is sensitive to random vibrations in its z-direction.

Figure 13 shows a similar result, as was seen from the sinusoidal vibration test: the IMU is insensitive to random vibrations in its X-axis.

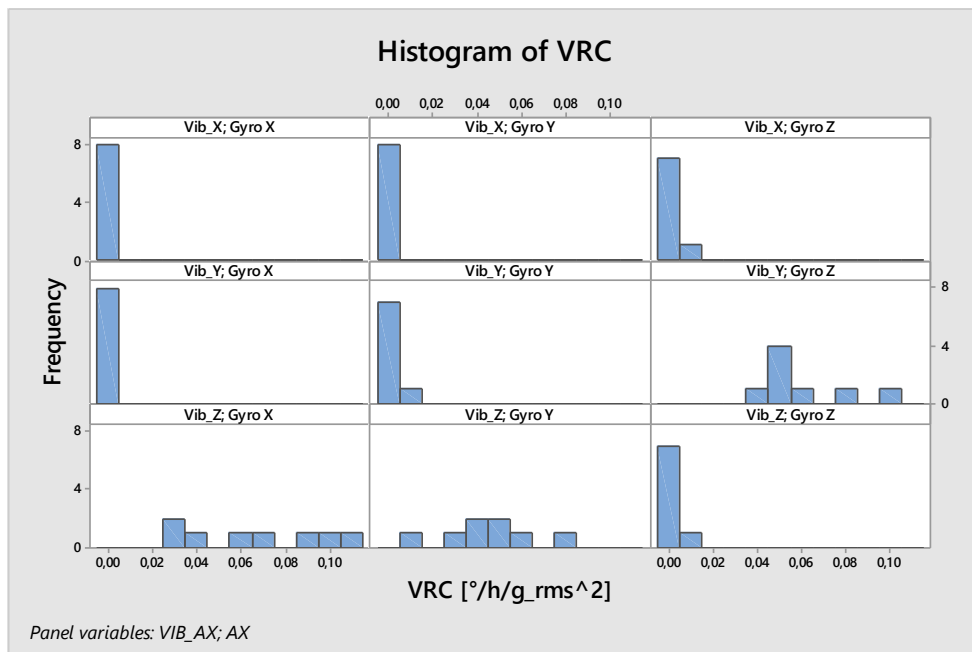


Figure 13: VRCs measured when applying random vibration in different directions

Figure 14 shows the cumulative distribution function (CDF)-plot for the VRC when vibration is applied in the vibration sensitive direction of the gyro sensing elements (z-axis). Mean + 1 sigma value has been marked in the plot:

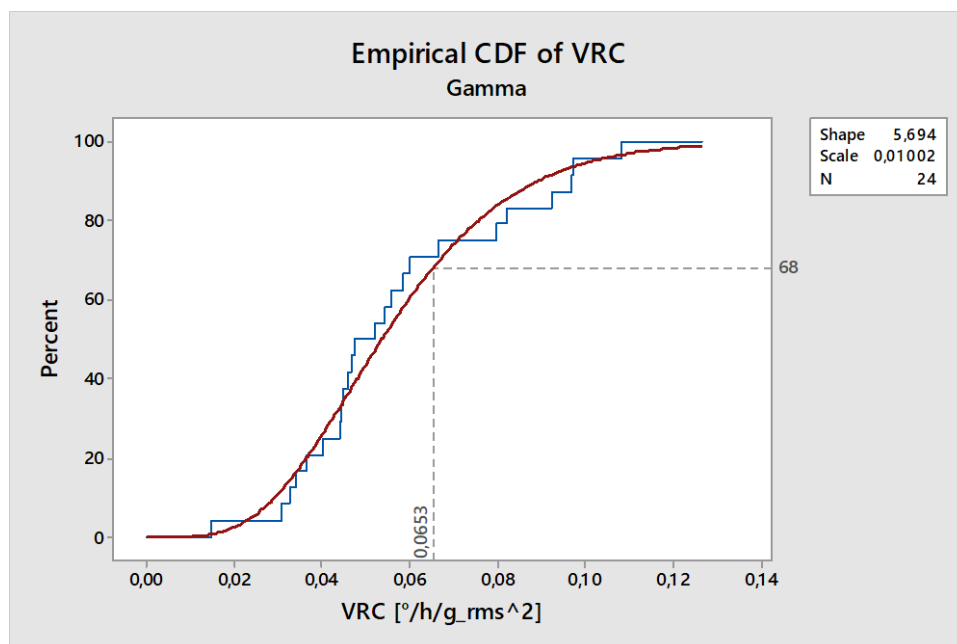


Figure 14: CDF of VRC when vibration is applied in the z-direction of the gyro sensing element

6. Mechanical Shock Tests

In this study, focus has been on the output of the continuous self-test – to investigate whether the shock is affecting the operation of the gyro. In addition, the gyro bias has been analyzed – to investigate whether a shift in bias can be observed after the shocks.

24 gyros (8 IMUs) were exposed to 5 consecutive mechanical shocks in 6 different axes directions; $\pm X$, $\pm Y$ and $\pm Z$ using 4 different profiles.

Overview shock profiles:

Test #	Amplitude [g]	Pulse length [ms]	Pulse Type	Number of shocks	Reference
1	40	15-23	Shock Response Spectrum (SRS)	5 x 6 directions	MIL-STD 810G CHG-1 method 516.7 "Functional Test for Ground Equipment & Crash Test for Flight Equipment", ref. figure 15
2	100	6	Half-sine	5 x 6 directions	
3	500	1.6	Half-sine	5 x 6 directions	
4	1500	0.5	Half-sine	5 x 6 directions	MIL-STD 883

Table 2: Mechanical shock test profiles

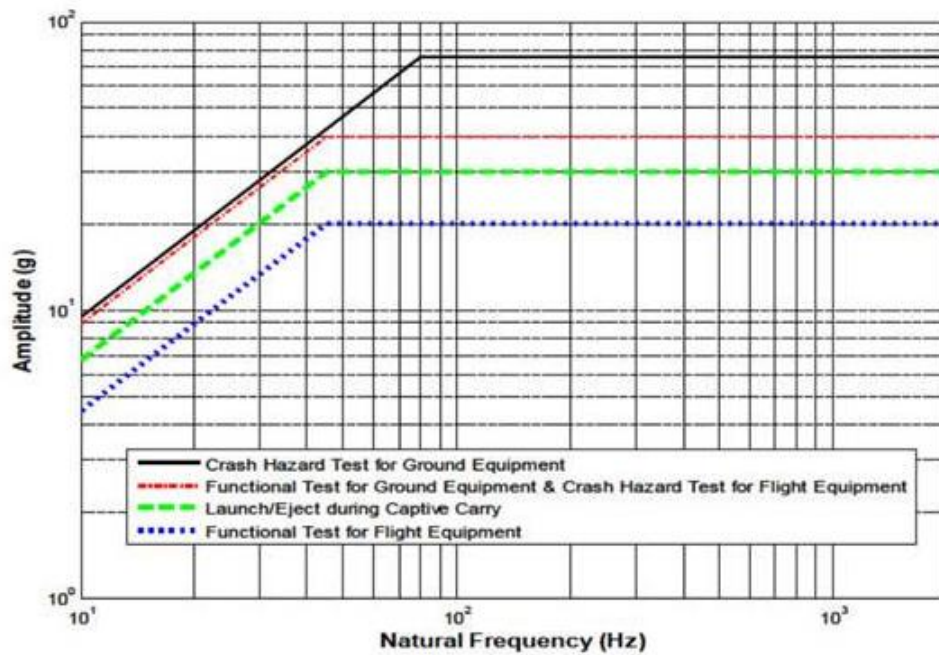


Figure 15: Specified spectrum for shock test#1

Tests #1 and #2 were performed using a shaker, set up to generate the required shock profile, as shown in figure 16:

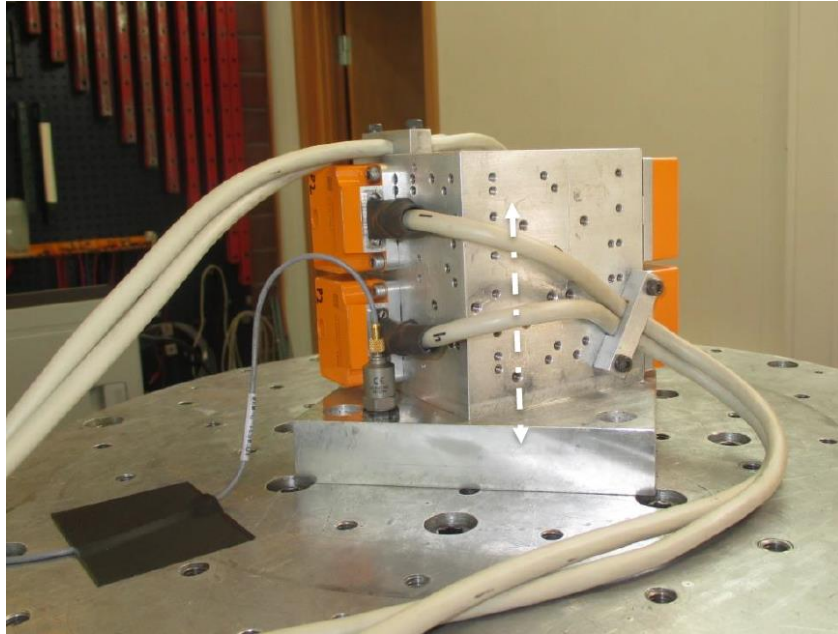


Figure 16: Test set-up for shock tests #1 and #2 (testing in y-direction)

Tests #3 and #4 were performed using a conventional shock tester, as shown in figure 17:



Figure 17: Test set-up for shock tests #3 and #4 (testing in z-direction)

The gyros were configured as follows:

- Range = $\pm 400^\circ/\text{s}$, output being clipped at $\pm 480^\circ/\text{s}$
- Sampling rate = 2000Hz
- Low-pass filter = 33Hz

Data transmission rate = 250Hz

Test Sequence:

- Start measurement sequence of approximately 4 minutes
- After approximately 2 minutes, apply 5 mechanical shocks
- Analyze relevant bits in status-register from continuous self-test
- Calculate bias shift from first 45s and last 45s

Figure 18 shows typical responses when exposing the parts to the defined shock profiles (note: different scaling on the y-axes):

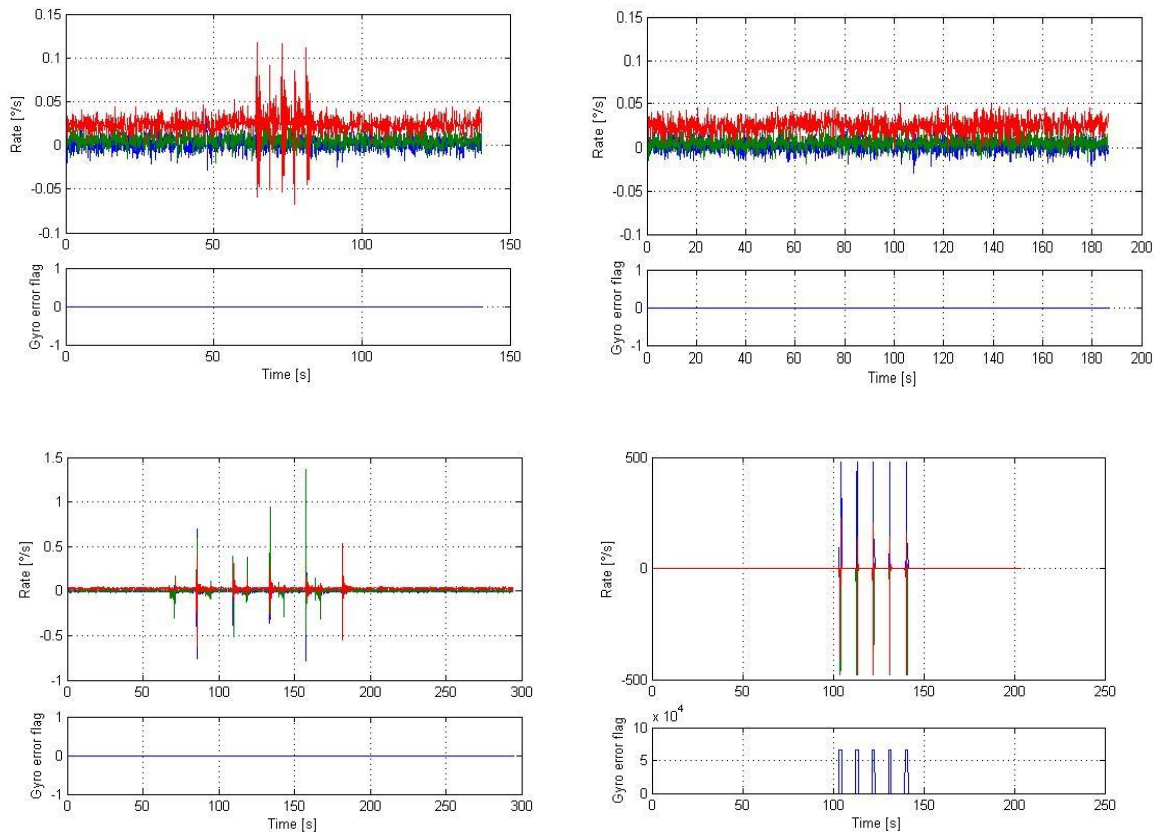


Figure 18: Response when being exposed to 40g (upper left), 100g (upper right), 500g (lower left) and 1500g (lower right) shocks in the y-axis

It is very difficult to evaluate and comment on the observed output of the gyros during shocking, especially at 500 and 1500g as these have been performed on a shock tester. These shocks are rather complex in nature, and it is difficult to differentiate e.g. rotations from g-forces without having access to precise and high-bandwidth instrumentation. In this study, the focus has been on whether the gyro functionality is being affected by the mechanical shocks and the possible effects on bias.

6.1 Continuous self-test of gyro during shock

Table 3 summarizes the number of times the gyro self-test was flagging an error:

	Number of shocks	Number of IMUs involved	Shock-directions involved
Shocks per shock-level	240	8 of 8	X(80), Y(80), Z(80)
Shocks with gyro self-test error flagging, 40g	0	0 of 8	
Shocks with gyro self-test error flagging, 100g	0	0 of 8	
Shocks with gyro self-test error flagging, 500g	5	2 of 8	X(2), Z(3)
Shocks with gyro self-test error flagging, 1500g	236	8 of 8	X(76), Y(80), Z(80)

Table 3: Overview of shocks with gyro self-test error flagging

As table 3 shows:

- No gyro error flagging was seen for any of the in total 480 shocks at 40g and 100g (8 IMUs seeing 30 shocks/g-level x 2 g-levels)
- At 500g, 2 IMUs experienced in total 5 shocks out of 60 with gyro error flagging. The remaining IMUs did not flag any errors in the gyro during the shocks
- At 1500g, all IMUs experienced gyro error flagging at almost every shock

Histograms of the duration of the gyro error flagging are shown in figure 19:

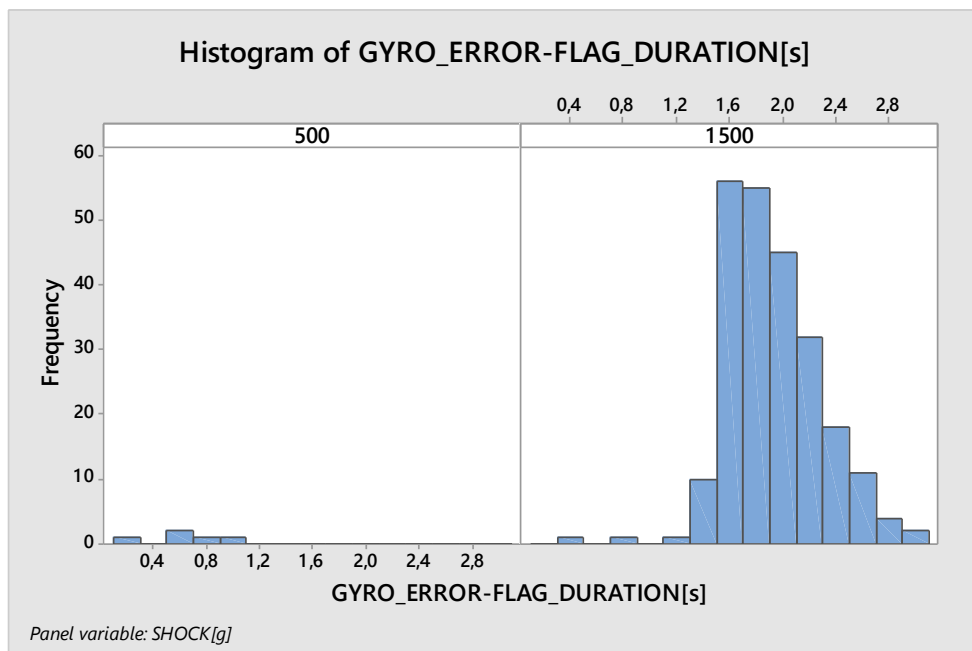


Figure 19: Duration of gyro error flagging

The duration of the gyro error-flagging for the few instances at 500g is clearly much shorter than the durations observed at 1500g. At 500g, the gyros are fully back in operation within 1 second. At 1500g it takes up to 3 seconds.

All 8 IMUs (24 axes) were exposed to the defined test program (120 shocks). In all cases where a gyro error flag was set during shock, the gyro error flag was reset after the shock, indicating no permanent damage to any of the gyros during the test program.

6.2 Bias-shift during shock

Histograms of bias-shifts for the 4 shock-profiles are shown in figure 20:

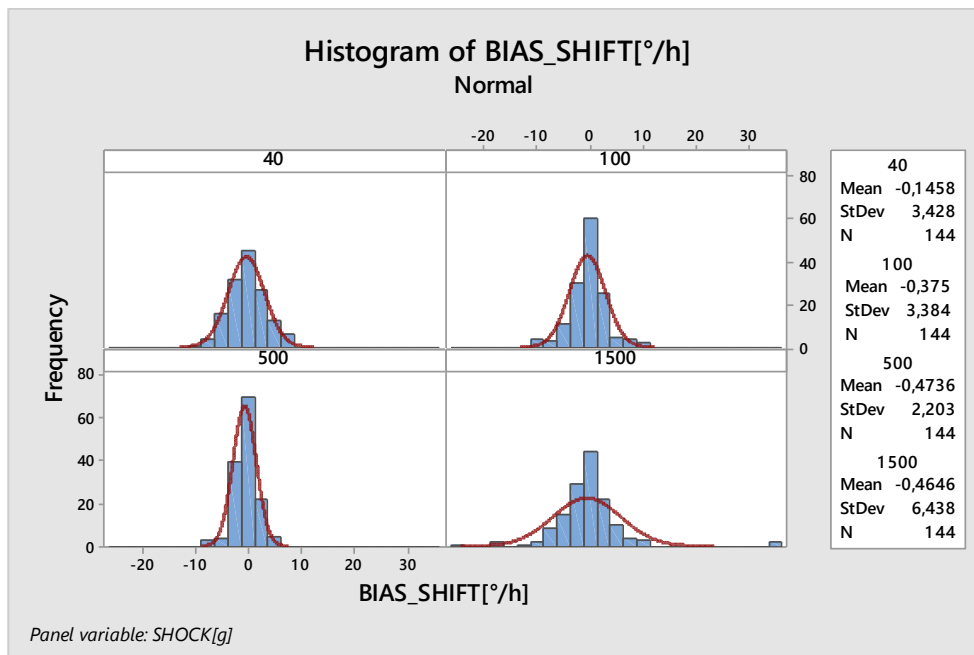


Figure 20: Histogram of bias-shifts during shocks

No shock profile results in any systematic shift in bias and there is no systematic shift related to the direction of the shock, as shown in figure 21:

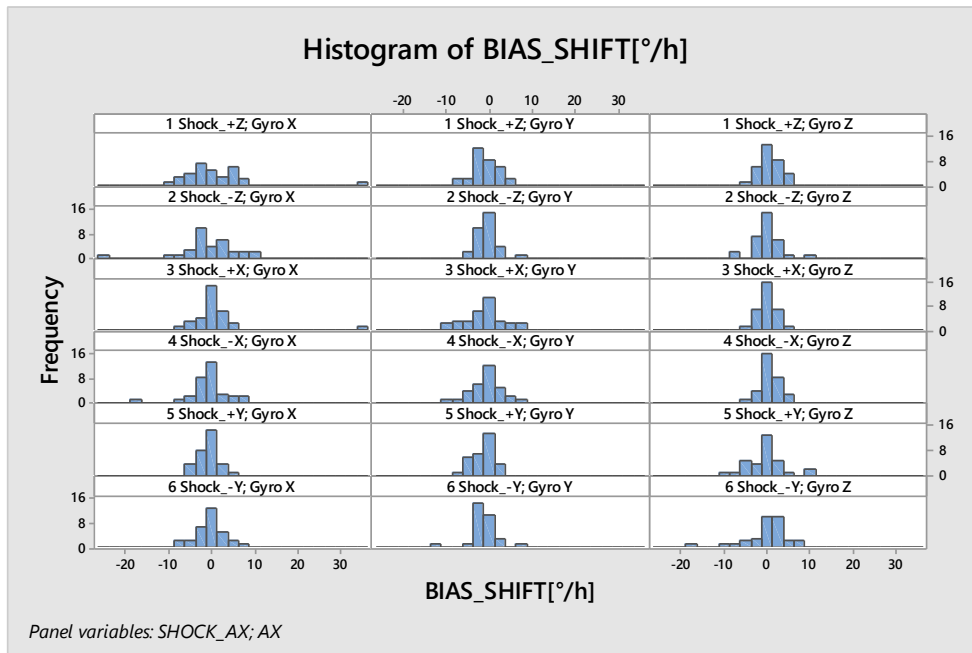


Figure 21: Bias-shifts during shocks in different directions

The observed spread in the data is within what to be expected. A few outliers (max. 35°/h) are observed at 1500g on the x-axis gyro. These are all related to one IMU as shown in figure 22:

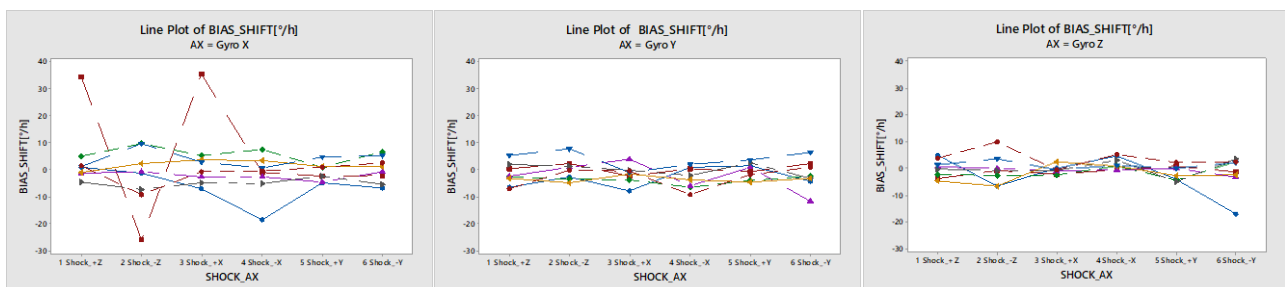


Figure 22: Bias shifts for gyros at 1500g shocks

The bias shifts in figure 22 show that 1 gyro out of 24 has a shift of 70°/h between two series of 5 shocks at 1500g. Keeping in mind that 1500g is at the maximum rating (survival) for the IMU and the observed shifts are well within the bias specifications, this demonstrates well the high robustness of the gyros.

7. Conclusions

7.1 *Sine and random vibration*

Measurements show that the gyro sensing element is sensitive to vibrations only in its z-direction. As a result of how the three gyros are mounted in the IMU, all gyros will be insensitive to vibrations in the x-direction of the IMU.

Applying the "High Performance Aircraft" random vibration profile resulted in a VRC of $0.06^\circ/\text{h}/\text{g}_{\text{rms}}^2$. This profile is dominated by frequencies in the 300-1000Hz range. The results from the sinusoidal vibrations match well, with a VRC of $0.02^\circ/\text{h}/\text{g}_{\text{rms}}^2$ at 500Hz and $0.07^\circ/\text{h}/\text{g}_{\text{rms}}^2$ at 1000Hz (all: mean + 1 sigma).

The vibration sensitivity up to 500Hz is below the measurement threshold.

The VRC [$^\circ/\text{h}/\text{g}_{\text{rms}}^2$] increases with increasing frequency and is constant in the g-range of 5-20g_{PEAK}.

7.2 *Mechanical Shock*

8 IMUs have each been exposed to 120 shocks including 4 shock profiles and shocking along all axes in both directions. No IMU showed sign of permanent damage after the shocking and the observed bias shifts, even when shocking at the maximum rating, were well within the specifications of the IMU.

During the shocks at 40g and 100g, all IMUs were fully functional. At 500g, 75% of the IMUs were fully functional. Only 2 of 24 gyros had in total 5 incidents out of 60 shocks where the continuous self-test flagged a gyro error. Hence the 500g shocks seem to be just above the level at which the gyros are fully functional during a mechanical shock.

At 1500g, all IMUs flagged a gyro error during the shocks. 1500g is at the specified maximum rating (survival). All IMUs returned to full function in less than only 3 seconds.